# Highlights

## Design-space Assessment and Dimensionality Reduction: An Off-line Method for Shape Reparameterization in Simulation-based Optimization

Danny D'Agostino,Andrea Serani,Matteo Diez

- Off-line methods allow for the assessment and dimensionality reduction of design spaces before shape optimization is performed.
- KLE/PCA based methods provide with a reparameterization of the shape modification vector for efficient optimization.
- The proposed method can be used with arbitrary shape parameterization/modification methods.
- Examples are given for the DTMB 5415 hull form optimization, using free-form deformation, radial basis functions, and global modification functions.

# Design-space Assessment and Dimensionality Reduction: An Off-line Method for Shape Reparameterization in Simulation-based Optimization

Danny D'Agostino[a,b], Andrea Serani[a] and Matteo Diez[a,*]

[a] CNR-INM, National Research Council–Institute of Marine Engineering, Rome, Italy

[b] Dept. of Computer, Control, and Management Engineering "A. Ruberti", Sapienza University of Rome, Italy

ARTICLE INFO

*Keywords*:
Shape parameterization
Design-space dimensionality reduction
Karhunen-Loève expansion
Principal component analysis
Simulation-based design optimization

ABSTRACT

A method based on the Karhunen-Loève expansion (KLE) is formulated for the assessment of arbitrary design spaces in shape optimization, assessing the shape modification variability and providing the definition of a reduced-dimensionality global model of the shape modification vector. The method is based on the concept of geometric variance and does not require design-performance analyses. Specifically, the KLE is applied to the continuous shape modification vector, requiring the solution of a Fredholm integral equation of the second kind. Once the equation is discretized, the problem reduces to the principal component analysis (PCA) of discrete geometrical data. The objective of the present work is to demonstrate how this method can be used to (a) assess different design spaces and shape parameterization methods before optimization is performed and without the need of running simulations for the performance prediction, and (b) reduce the dimensionality of the design space, providing a shape reparameterization using KLE/PCA eigenvalues and eigenmodes. A demonstration for the hull-form optimization of the DTMB 5415 model in calm water is shown, where three design spaces are investigated, namely provided by free-form deformation, radial basis functions, and global modification functions of the hull.

## 1. Introduction

The simulation-based design (SBD) paradigm has demonstrated the capability of supporting ship designers and marine/ocean engineers, not only providing large sets of design options but also exploring operational spaces by assessing the design performance for a large number of operating and environmental conditions. The recent development of high performance computing (HPC) systems has driven the SBD towards integration with global optimization (GO) algorithms and uncertainty quantification (UQ) methods, moving the SBD paradigm to automatic deterministic and stochastic SBD optimization (SBDO, Campana et al. 2006; Diez et al. 2018b,c) and simulation-driven (SDD, Harries and Abt 2019) formulations, possibly aiming at global solutions to the design problem. In shape design, SBDO consists of three main elements as shown in Fig. 1 (see right box): (i) a deterministic and/or stochastic simulation tool (integrating physics-based solvers with UQ), (ii) an optimization algorithm, and (iii) a shape modification tool.

Despite the increased computational power and robustness of numerical algorithms, high-fidelity SBDO for shape optimization still remains a challenging process, from theoretical, algorithmic, and technological viewpoints. Among others, one of the most complex challenge is how to deal with high-dimensional, large design spaces, especially when computationally-expensive black-box functions are used for the performance analysis and a global optimum is sought after. Potential design improvements significantly depend on dimension and extension of the design space. Obviously, high dimension and variability spaces are more difficult and expensive to explore but, at the same time, potentially allow for bigger improvements. Even if efficient GO algorithms have been proposed (Jones et al., 1993; Campana et al., 2009a; Serani and Diez, 2017b) and applied with success to SBDO (Campana et al., 2015; Serani et al., 2016a; Serani and Diez, 2018a), finding a potentially global optimal solution within reasonable computational time/cost remains a critical issue and a technological challenge. Additionally, UQ of complex applications is computationally very demanding, especially if high-order statistical moments and/or quantiles need to be assessed as in robust and reliability-based design optimization. Both global optimization and UQ are affected by the *curse of dimensionality* as the algorithms' complexity and computational cost rapidly increase with the problem dimension. This is generally also true if metamodels are applied. Therefore, the assessment and breakdown of the design-space dimensionality are key elements for the efficiency and affordability of the SBDO (Diez et al., 2015a).

In this context, shape optimization research has traditionally focused on shape and topology parameteri-

*Corresponding author
matteo.diez@cnr.it (M. Diez)
www.inm.cnr.it (M. Diez)
ORCID(s): 0000-0002-8814-1793 (A. Serani); 0000-0001-6113-7893 (M. Diez)

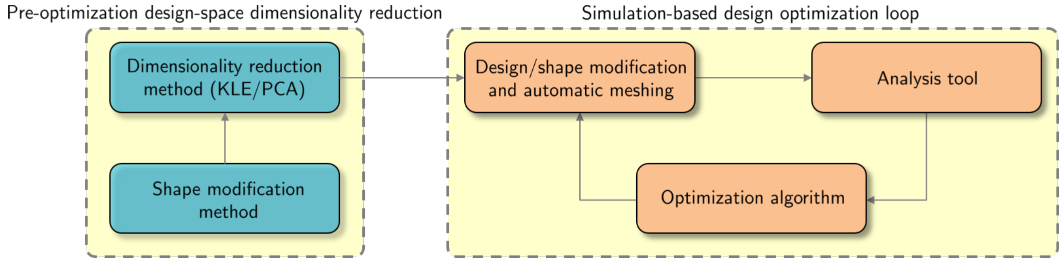


**Figure 1:** SBDO framework with off-line design-space dimensionality reduction.

zations, as critical factors to achieve the desired level of design variability (Rozvany et al., 1992; Bletzinger and Maute, 1997; Samareh, 2001). Obviously, the choice of the shape parameterization technique has a large impact on the practical implementation and the success of the optimization process. Shape deformation methods have been an area of continuous and extensive research within the fields of computer graphics and geometry modelling. Consequently, a wide variety of techniques has been proposed during recent years (Sieger et al., 2015). Several techniques have been developed and applied (Samareh, 2001), such as: basis vector methods (Pickett Jr. et al., 1973), domain element and discrete approaches (Leiva and Watson, 1998), partial differential equation (Bloor and Wilson, 1995), CAD-based (Yang, 1995), analytical (Hicks and Henne, 1978), polynomials (Haftka and Grandhi, 1986), B-splines (Grigoropoulos and Chalkias, 2010), non-uniform rational Bezier-spline (NURBS), patches of Bezier surfaces (Campana et al., 2006), free-form deformation (FFD, Sederberg and Parry 1986), and morphing approaches (Kandasamy et al., 2013). In order for the SBDO to avoid the curse of dimensionality and be successful, the parameterization method must efficiently describe the design variability with as few variables as possible. However, in most of past SBDO literature, the trade-off between geometric variability and design space dimensionality is not directly/quantitatively addressed or only qualitatively assessed.

In order to solve complex and computationally-demanding optimization problems, on-line linear design-space dimensionality reduction techniques have been developed, requiring the evaluation of the objective function or its gradient. Principal component analysis (PCA) or proper orthogonal decomposition (POD) methods have been applied for local reduced-dimensionality representations of feasible design regions (Raghavan et al., 2013a,b). The associated POD/PCA-based expansions are not truncated and the dimensionality reduction is achieved by a local representation of an $\alpha$-manifold of feasible designs, embedding therefore the design constraints (whose evaluation is required) in the design parameterization and preserving the original design variability. A PCA/POD-based approach is used in the active subspace method (Lukaczyk et al., 2014) to discover and exploit low-dimensional monotonic trends in the objective function, based on the evaluation of its gradient. This type of methods improve the optimization efficiency by basis rotation and/or dimensionality reduction. Nevertheless, they do not provide an assessment of the design space and associated shape parameterization before optimization is performed or objective function and/or gradient are evaluated. Moreover, if gradients are not directly provided (as in the case of black-box tools) their evaluation by finite differences can be inaccurate due to numerical noise and/or residuals affecting the solution. Finally, these methods are local in nature and their extension to GO is not trivial nor straightforward.

Off-line (or up-front) linear models have been developed with focus on design-space variability and dimensionality reduction for efficient optimization procedures. In Borzì et al. (2010) and Schillings et al. (2011) the Karhunen-Loève expansion (KLE, equivalent to POD) is used for representing distributed geometrical uncertainties and building a reduced-order spatial model for uncertainty quantification. A method based on the KLE has been formulated in Diez et al. (2015a) for the assessment of the shape modification variability and the definition of a reduced-dimensionality global model of the shape modification vector, for arbitrary modification methods. No objective function evaluation nor gradient is required by the method, as this is entirely based on the concept of geometric variance. KLE is formulated in the continuous domain and reduces to the eigenproblem of an integral operator, representing a Fredholm integral equation of the second kind. The discretization of the shape domain (and associated integral equation) yields the eigenproblem of a matrix, which appears to be the autocovariance matrix of the discretized shape modification vector. This corresponds to solving the PCA of the discretized shape modification vector. KLE/PCA methods have been successfully applied for deterministic (Chen et al., 2015; Diez et al., 2016a; Serani et al., 2016a) and stochastic (Diez et al., 2015b, 2018a) hull form optimization of mono-hulls and catamarans in calm water and waves, respectively. Similarly, Poole et al. (2017) have applied POD to airfoil shape optimization via singular value decomposition (SVD) of an airfoil geometric-data library. Off-line methods improve the shape optimization efficiency by reparameterization and dimensionality reduction, providing the assessment of the design space and the shape parameterization before optimization and/or performance analysis are carried out. The assessment is based on the geometric variability associated to the design space, making the method fully off-line and computationally very efficient and attractive, as no simulations are required. Theory and mathematical derivation of design variability breakdown, associated confidence levels, and dimensionality reduction for hydrodynamic shape optimization still remain limited. Applications to ship hydrodynamic optimization are also limited.

The objective of the present work is to demonstrate how off-line KLE/PCA methods based on the concept on geometric variance can be used to assess different design spaces and shape parameterization methods before optimization is performed and without needing to run simulations for the design performance prediction. The method is further exploited to reduce the dimensionality of the design spaces (based on the KLE/PCA eigenvalues), providing an efficient shape reparameterization using KLE/PCA eigenmodes.

The approach is shown in Fig. 1. The left box includes the elements of the geometry-based formulation of the pre-optimization (off-line) design-space dimensionality reduction method. The right box represents a typical optimization loop including shape modification, analysis tool (e.g., computational fluid dynamics, finite element analysis, possibly coupled with UQ), and optimization algorithm, whose detailed description is beyond the scope of the current work. The method is demonstrated for the hull-form optimization of the DTMB 5415 model, an early and open to public version of the USS Arleigh Burke destroyer DDG 51, extensively used as an international benchmark for shape optimization problems (e.g., Diez et al. 2018b,c). The optimization aims at the reduction of the (model-scale) calm-water resistance at Froude number equal to 0.28. Simulations are based on a potential flow code with viscous correction. Three design spaces are investigated, namely provided by FFD, radial basis functions (RBF), and global modification functions (GMF). It may be noted that the objective of the investigation is not the comparison of different shape modification methods *per se*, but the demonstration of how KLE/PCA can be used to assess and compare different design spaces provided by arbitrary modification methods. An example of comparison by KLE/PCA of design spaces defined using the same modification method (namely FFD) is given in Diez et al. (2015a).

## 2. Dimensionality Reduction Method

General definitions and assumptions for design-space assessment and dimensionality reduction are presented in the following. For further details on the theory and implementation, the interested reader is referred to Diez et al. (2015a).

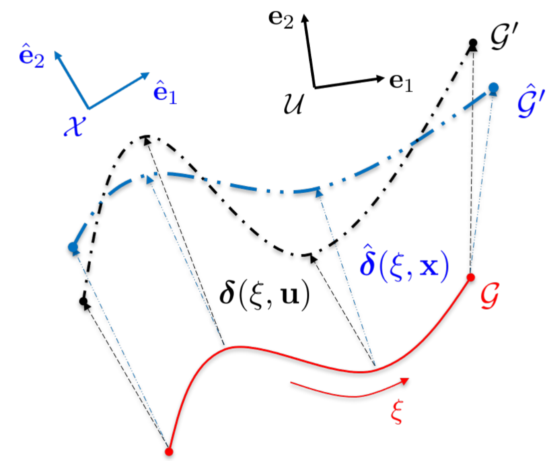


**Figure 2:** Scheme and notation for the current formulation.

### 2.1. General Definitions and Assumptions

Consider a geometric domain $\mathcal{G}$ (which identifies the original or parent shape) and a set of coordinates $\boldsymbol{\xi} \in \mathcal{G} \subset \mathbb{R}^n$ with $n = 1, 2, 3$. Assume that $\mathbf{u} \in \mathcal{U} \subset \mathbb{R}^M$ is the design-variable vector, which defines a continuous shape modification vector $\boldsymbol{\delta}(\boldsymbol{\xi}, \mathbf{u}) \in \mathbb{R}^m$ with $m = 1, 2, 3$ (with $m$ not necessarily equal to $n$). Each $\boldsymbol{\xi} \in \mathcal{G}$ is transformed in $\boldsymbol{\xi}' \in \mathcal{G}'$ as

$$\boldsymbol{\xi}' = \boldsymbol{\xi} + \boldsymbol{\delta}(\boldsymbol{\xi}, \mathbf{u}) \tag{1}$$

where $\mathcal{G}$ and $\mathcal{G}'$ represent the original and modified shapes respectively (see Fig. 2).

Consider $\mathbf{u}$ as a random variable, with associated probability density function $p(\mathbf{u})$. This corresponds to formulating the optimization problem as a problem affected by *epistemic uncertainty*, in the sense that before solving the problem, the optimal solution is yet unknown. In this context, the distribution $p(\mathbf{u})$ represents the prior probability of finding an optimal solution in a given region of the design space. Although its definition can be based on experience and/or earlier studies, it is often not trivial and therefore the prior is usually defined as a uniform distribution function (therefore giving each point in the design space the same probability to be an optimal solution). The mean shape modification associated to $p(\mathbf{u})$ is

$$\langle \boldsymbol{\delta} \rangle = \int_{\mathcal{U}} \boldsymbol{\delta}(\boldsymbol{\xi}, \mathbf{u}) p(\mathbf{u}) \mathrm{d}\mathbf{u} \tag{2}$$

whereas the variance associated to the shape modification vector (geometric variance) is defined as

$$\sigma^2 = \langle \|\boldsymbol{\delta}\|^2 \rangle = \int_{\mathcal{U}} \int_{\mathcal{G}} \tilde{\boldsymbol{\delta}}(\boldsymbol{\xi}, \mathbf{u}) \cdot \tilde{\boldsymbol{\delta}}(\boldsymbol{\xi}, \mathbf{u}) p(\mathbf{u}) \mathrm{d}\boldsymbol{\xi} \mathrm{d}\mathbf{u} \tag{3}$$

where $\widetilde{\boldsymbol{\delta}} = \boldsymbol{\delta} - \langle \boldsymbol{\delta} \rangle$. For the sake of simplicity and without loss of generality, in the following it is assumed $\langle \boldsymbol{\delta} \rangle = 0$ and $\widetilde{\boldsymbol{\delta}} = \boldsymbol{\delta}$.

### 2.2. Aim of Dimensionality Reduction and Evaluation Metrics

Within this framework, the aim of the dimensionality reduction is to identify an approximated representation of the shape modification vector, namely $\hat{\boldsymbol{\delta}}(\boldsymbol{\xi}, \mathbf{x})$, for which its shape modification depends on a new reduced-dimensionality design variable $\mathbf{x} \in \mathcal{X} \subset \mathbb{R}^N$ with $N < M$. In general, the reconstructed vector $\hat{\boldsymbol{\delta}}(\boldsymbol{\xi}, \mathbf{x})$ is estimated during a process of encoding/decoding by the dimensionality reduction methods. The shape modification vector $\boldsymbol{\delta}(\boldsymbol{\xi}, \mathbf{u})$ is encoded in a low dimensional latent space, spanned by a new design variable $\mathbf{x}$. Subsequently, the decoding process reconstructs the original shape modification vector as $\hat{\boldsymbol{\delta}}(\boldsymbol{\xi}, \mathbf{x})$. Figure 2 shows an example with the notation for $n = 1$ and $m = 2$.

A common metrics to evaluate the quality of $\hat{\boldsymbol{\delta}}(\boldsymbol{\xi}, \mathbf{x})$ compared to $\boldsymbol{\delta}(\boldsymbol{\xi}, \mathbf{u})$ is the mean squared error (MSE) normalized to the total geometric variance ($\sigma^2$) as

$$\mathrm{NMSE} = \frac{\mathrm{MSE}}{\sigma^2} = \frac{\iint\limits_{\mathcal{U}\times\mathcal{X},\mathcal{G}} \|\boldsymbol{\delta}(\boldsymbol{\xi}, \mathbf{u}) - \hat{\boldsymbol{\delta}}(\boldsymbol{\xi}, \mathbf{x})\|^2 p(\mathbf{u}, \mathbf{x}) \mathrm{d}\boldsymbol{\xi} \mathrm{d}\mathbf{u} \mathrm{d}\mathbf{x}}{\iint\limits_{\mathcal{U},\mathcal{G}} \|\boldsymbol{\delta}(\boldsymbol{\xi}, \mathbf{u})\|^2 p(\mathbf{u}) \mathrm{d}\boldsymbol{\xi} \mathrm{d}\mathbf{u}} \tag{4}$$

where $p(\mathbf{u}, \mathbf{x})$ is an unknown joint probability distribution over the product space $\mathcal{U} \times \mathcal{X}$.

### 2.3. Karhunen-Loève Expansion and Principal Component Analysis

At the continuous level, an optimal linear representation of the shape modification vector is provided by its KLE (Diez et al., 2015a), as

$$\hat{\boldsymbol{\delta}}(\boldsymbol{\xi}, \mathbf{x}) = \sum_{i=1}^{N} x_i \boldsymbol{\varphi}_i(\boldsymbol{\xi}) \tag{5}$$

where $\boldsymbol{\varphi}_i$ are the eigensolutions of the Fredholm integral equation of the second kind

$$\int_{\mathcal{G}} \langle \boldsymbol{\delta}(\boldsymbol{\xi}, \mathbf{u}) \otimes \boldsymbol{\delta}(\boldsymbol{\psi}, \mathbf{u}) \rangle \boldsymbol{\varphi}(\boldsymbol{\psi}) \mathrm{d}\boldsymbol{\psi} = \lambda \boldsymbol{\varphi}(\boldsymbol{\xi}) \tag{6}$$

Discretizing $\mathcal{G}$ by a number of $Q$ elements of equal measure $\Delta\mathcal{G}$, assuming for the sake of simplicity and without loss of generality $\Delta\mathcal{G} = 1$, and sampling $\mathcal{U}$ by a statistically convergent number of Monte Carlo (MC) realizations $S$, so that $\{\mathbf{u}_k\}_{k=1}^S \sim p(\mathbf{u})$. The spatial discretization $\mathbf{d}(\mathbf{u})_k$ of $\boldsymbol{\delta}(\boldsymbol{\xi}, \mathbf{u}_k)$ are organized in a $[S \times L]$ data matrix as

$$\mathbf{D} = \begin{bmatrix} \mathbf{d}(\mathbf{u})_{k=1}^\mathsf{T} \\ \vdots \\ \mathbf{d}(\mathbf{u})_{k=S}^\mathsf{T} \end{bmatrix} \tag{7}$$

where $L = mQ$. To simplify the notation, in the following $\mathbf{d}(\mathbf{u})$ and $\hat{\mathbf{d}}(\mathbf{x})$ are referred to as simply $\mathbf{d}$ and $\hat{\mathbf{d}}$, respectively.

At the discrete level, the integral problem in Eq. 6 reduces to solving the PCA of $\mathbf{D}$. The principal components are defined by the solution of the eigenproblem

$$\mathbf{C}\mathbf{z}_i = \lambda_i \mathbf{z}_i \qquad \forall i = 1, \dots, L \tag{8}$$

where

$$\mathbf{C} = \frac{1}{S}\mathbf{D}^\mathsf{T}\mathbf{D} \tag{9}$$

is the $[L \times L]$ covariance matrix. PCA allows to reduce the input dimensionality of the data, performing a projection of data points in a new linear subspace, defined by the orthonormal eigenvectors (principal components) of $\mathbf{C}$. These eigenvectors have the properties of maximizing the (geometric) variance of points projected on them and minimizing the mean squared distance between the original points and the relative projections. Moreover, the eigenvalues $\{\lambda_i\}_{i=1}^L$ (with $\lambda_i \geq \lambda_{i+1}$) represent the variance resolved along the associate eigenvectors $\{\mathbf{z}_i\}_{i=1}^L$. Additionally,

$$\sigma^2 = \sum_{i=1}^{\infty} \lambda_i \tag{10}$$

From this property, a subset of $N$ eigenvectors is used to compute a reduced-dimensionality representation of the original vector $\mathbf{d}$ as

$$\hat{\mathbf{d}}_k = \mathbf{Z}\mathbf{x}_k \tag{11}$$

where the matrix $\mathbf{Z}$ has dimension $[L \times N]$ and is composed by the first $N$ largest-variance principal components. Equation 11 represents the desired reparameterization of the shape modification vector by KLE/PCA where $\hat{\mathbf{d}}_k$ represents the minimum-squared-error approximation of $\mathbf{d}_k$ and the new design variables $\mathbf{x}_k$ are given by

$$\mathbf{x}_k = \mathbf{Z}^\mathsf{T}\mathbf{d}_k \tag{12}$$

The discrete form of the NMSE in Eq. 4 reads

$$\mathrm{NMSE} = \frac{\frac{1}{S}\sum_{k=1}^S ||\mathbf{d}_k - \hat{\mathbf{d}}_k||^2}{\frac{1}{S}\sum_{k=1}^S ||\mathbf{d}_k||^2} = \frac{\frac{1}{S}\sum_{k=1}^S ||\mathbf{d}_k||^2 - \sum_{i=1}^N \mathbf{z}_i^\mathsf{T}\mathbf{C}\mathbf{z}_i}{\frac{1}{S}\sum_{k=1}^S ||\mathbf{d}_k||^2} \tag{13}$$

which holds if one uses either a validation set or the training set for the assessment. In the latter case, Eq. 13 can be written as

$$\mathrm{NMSE} = 1 - \frac{\sum_{i=1}^N \lambda_i}{\frac{1}{S}\sum_{k=1}^S ||\mathbf{d}_k||^2} \tag{14}$$

It may be noted that in principle Eqs. 7-14 still hold if data standardization is used, i.e. if a data matrix with unit-variance columns is processed. Although this is a standard procedure to analyze heterogeneous and discrete data with PCA and/or non-supervised machine learning methods, this would change the Hilbert space (and the associated norm) embedding the analysis and the definition of geometric variance in Eq. 3, modifying the key metrics the dimensionality reduction is based upon (Diez et al., 2015a). As a consequence, the resulting reduced-dimensionality representation of $\boldsymbol{\delta}$ would not be optimal anymore to resolve the geometric variance associated to the original design space. In this regard, Eqs. 7-14 for discrete data derive directly from Eqs. 1 -6 defined for continuous variables. In particular, PCA (Eq. 8) is the discrete counterpart of KLE integral equation (Eq. 6). Therefore, data and covariance matrices should not be standardized if an approximate (discrete) solution of Eq. 6 is sought after. Equations and examples of the use of generalized Hilbert spaces (at the continuous level) are given in Diez et al. (2015a).

## 3. Shape Modification Methods

It is often convenient in the context of SBDO to apply shape modification methods that allow also for the modification of the computational grid, without need for regridding from scratch. This usually overcomes the difficulties and bottle necks associated to regridding of new designs (Sieger et al., 2014). Modification methods that modify not only the object shape, but also the space embedding the object, usually allows for automatic grid modification: (1) the grid has not to be regenerated from scratch each time the object shape is modified, (2) the initial topology is usually preserved, and (3) parts of the object can be deformed with a prescribed degree of continuity.

Here, three common approaches to shape and grid modification are applied as described in the following. These methods are suitable candidates for demonstrating shape reparameterization by KLE/PCA since they allow for the use of a possibly infinite number of design variables.

### 3.1. Free-form Deformation

FFD has been widely used in many technological fields (Menzel and Sendhoff, 2008; Campana et al., 2009b; Diez et al., 2015a; Chen et al., 2015). The technique was first described in Sederberg and Parry (1986) and is based on an earlier study described in Barr (1984). The idea is to embed an object within a trapezoidal (or other topology) lattice and modify the object within the trapezoid as the lattice is modified. A coordinate system is assumed, with origin $\boldsymbol{\xi}_0$ at one of the trapezoid vertices. Any point within the trapezoid has $\alpha$, $\beta$, and $\gamma$ coordinates such that

$$\boldsymbol{\xi} = \boldsymbol{\xi}_0 + \alpha\hat{\mathbf{T}}_1 + \beta\hat{\mathbf{T}}_2 + \gamma\hat{\mathbf{T}}_3 \tag{15}$$

with $\alpha$, $\beta$, and $\gamma$ bounded by $[0,1]$ and given by

$$\alpha = \frac{\hat{\mathbf{T}}_2 \times \hat{\mathbf{T}}_3 \cdot (\boldsymbol{\xi} - \boldsymbol{\xi}_0)}{\hat{\mathbf{T}}_2 \times \hat{\mathbf{T}}_3 \cdot \hat{\mathbf{T}}_1},$$

$$\beta = \frac{\hat{\mathbf{T}}_1 \times \hat{\mathbf{T}}_3 \cdot (\boldsymbol{\xi} - \boldsymbol{\xi}_0)}{\hat{\mathbf{T}}_1 \times \hat{\mathbf{T}}_3 \cdot \hat{\mathbf{T}}_2},$$

$$\gamma = \frac{\hat{\mathbf{T}}_1 \times \hat{\mathbf{T}}_2 \cdot (\boldsymbol{\xi} - \boldsymbol{\xi}_0)}{\hat{\mathbf{T}}_1 \times \hat{\mathbf{T}}_2 \cdot \hat{\mathbf{T}}_3} \tag{16}$$

Control points (CPs) $\mathbf{c}_{ijk}$ are defined as lattice nodes. The number of CPs used in $\hat{\mathbf{T}}_1$, $\hat{\mathbf{T}}_2$, and $\hat{\mathbf{T}}_3$ directions are $t_1$, $t_2$, and $t_3$, respectively. The coordinates of modified CPs depend on the original-lattice nodes and the design variable vector, as

$$\mathbf{c}_{ijk}(\mathbf{u}) = \boldsymbol{\xi}_0 + \frac{i}{t_1}\hat{\mathbf{T}}_1 + \frac{j}{t_2}\hat{\mathbf{T}}_2 + \frac{k}{t_3}\hat{\mathbf{T}}_3 + \mathbf{u}_{ijk} \tag{17}$$

The shape modification is achieved by interpolating the CPs' modification over the embedding space. The interpolation can be performed using different polynomial bases. Herein, a tensor product of trivariate Bernstein polynomial is used (Sederberg and Parry, 1986)

$$\boldsymbol{\delta}(\boldsymbol{\xi}, \mathbf{u}) = \sum_{i=0}^{t_1}\sum_{j=0}^{t_2}\sum_{k=0}^{t_3} b_{i,t_1}(\alpha) b_{j,t_2}(\beta) b_{k,t_3}(\gamma) \mathbf{c}_{ijk}(\mathbf{u}) - \boldsymbol{\xi} \tag{18}$$

where the generic Bernstein basis polynomials is defined as

$$b_{v,r}(\chi) = \binom{r}{v} \chi^v (1-\chi)^{r-v} \tag{19}$$

On the one hand, the FFD can be applied to any computational-grid topology and is suitable for a variety of analysis codes. On the other hand, the variables associated to the CPs' modification may have little or no physical meaning to the design engineers, thereby making it difficult to define an effective design space.

### 3.2. Radial Basis Function

The shape modification is defined starting from given modifications at specified CPs, which are usually nodes of the (discretized) object surface. The RBF interpolation is based on three sets of coordinates: original and modified CPs ($\mathbf{c}_j$ and $\mathbf{c}'_j(\mathbf{u}) = \mathbf{c}_j + \mathbf{u}_j$, respectively), surface nodes $\{\boldsymbol{\xi}_i\}_{i=1}^{Q}$ of the original discretized shape, and additional conditions if necessary. The goal is to find updated surface node positions all over the whole geometry. Treating the shape modification problem as a scattered data interpolation problem, the shape modification function $\boldsymbol{\delta}(\boldsymbol{\xi},\mathbf{u})$ exactly interpolates the prescribed displacements at a given CP ($\mathbf{u}_i$), and smoothly interpolates these displacements onto the geometry.

The shape modification function is defined as a linear combination of radially-symmetric kernel functions $\varphi_j(\boldsymbol{\xi}) = \varphi(\|\boldsymbol{\xi}-\mathbf{c}_j\|)$ centered in $\mathbf{c}_j$ and weighted by $\mathbf{w}_j \in \mathbb{R}^3$, plus a linear polynomial to guarantee linear precision such that

$$\boldsymbol{\delta}(\boldsymbol{\xi},\mathbf{u}) = \sum_{j=1}^{M} \mathbf{w}_j \varphi_j(\boldsymbol{\xi}) + \sum_{k=1}^{4} \mathbf{q}_k \pi_k(\boldsymbol{\xi}) \tag{20}$$

where $\{\pi_1,\pi_2,\pi_3,\pi_4\} = \{\xi_1,\xi_2,\xi_3,1\}$ is a basis of the space of linear trivariate polynomials, weighted by coefficients $\mathbf{q}_k \in \mathbb{R}^3$ (Sieger et al., 2014). The weights $\mathbf{w}_j$ and $\mathbf{q}_k$ are found imposing $\boldsymbol{\xi}_j = \mathbf{c}_j$ and solving the $(M+4)\times(M+4)$ linear system

$$\mathbf{AW} = \mathbf{B} \tag{21}$$

where

$$\mathbf{A} = \begin{bmatrix} \varphi_1(\mathbf{c}_1) & \dots & \varphi_M(\mathbf{c}_1) & \pi_1(\mathbf{c}_1) & \dots & \pi_4(\mathbf{c}_1) \\ \vdots & \ddots & \vdots & \vdots & \ddots & \vdots \\ \varphi_1(\mathbf{c}_M) & \dots & \varphi_M(\mathbf{c}_M) & \pi_1(\mathbf{c}_M) & \dots & \pi_4(\mathbf{c}_M) \\ \pi_1(\mathbf{c}_1) & \dots & \pi_1(\mathbf{c}_M) & 0 & \dots & 0 \\ \vdots & \ddots & \vdots & \vdots & \ddots & \vdots \\ \pi_4(\mathbf{c}_1) & \dots & \pi_4(\mathbf{c}_M) & 0 & \dots & 0 \end{bmatrix};$$

$$\mathbf{W} = [\mathbf{w}_1,\dots,\mathbf{w}_M,\mathbf{q}_1,\dots,\mathbf{q}_4]^{\mathsf{T}};$$

$$\mathbf{B} = [\mathbf{u}_1,\dots,\mathbf{u}_M,0,\dots,0]^{\mathsf{T}} \tag{22}$$

The shape of the interpolant is determined by the choice of the kernel function $\varphi:\mathbb{R}\to\mathbb{R}$. Commonly used kernel includes Gaussian, multiquadric, and inverse mutiquadric, as summarized in Tab. 1.

**Table 1**
Commonly used kernel functions for RBF interpolation. $\epsilon$ is the shape parameter.

| Kernel | Equation |
|---|---|
| Gaussian | $\varphi(\boldsymbol{\xi}) = e^{-(\epsilon\,\boldsymbol{\xi})^2}$ |
| Multiquadric | $\varphi(\boldsymbol{\xi}) = \sqrt{1+(\epsilon\,\boldsymbol{\xi})^2}$ |
| Inverse Multiquadric | $\varphi(\boldsymbol{\xi}) = 1/\sqrt{1+(\epsilon\,\boldsymbol{\xi})^2}$ |

RBF can be applied on the whole object or a part of it. Moreover, the associated design variables can be related to a physical meaning, since CPs' displacement is directly related to the shape modification in that regions.

### 3.3. Global Modification Function

The shape modification $\boldsymbol{\delta}(\boldsymbol{\xi},\mathbf{u})$ is defined using a linear combination of $M$ vector-valued functions of the Cartesian coordinates $\boldsymbol{\xi}\in\mathbb{R}^3$ over a hyper-rectangle embedding the object (Serani et al., 2016a)

$$\boldsymbol{\phi}_i(\boldsymbol{\xi}) \;:\; \mathcal{V} = [0,L_{\xi_1}]\times[0,L_{\xi_2}]\times[0,L_{\xi_3}] \in \mathbb{R}^3 \longrightarrow \mathbb{R}^3 \tag{23}$$

with $i = 1,...,M$, as

$$\boldsymbol{\delta}(\boldsymbol{\xi},\mathbf{u}) = \sum_{i=1}^{M} u_i\,\boldsymbol{\phi}_i(\boldsymbol{\xi}) \tag{24}$$

where the coefficients $u_i \in \mathbb{R}$ ($i=1,\dots,M$) are the design variables and

$$\boldsymbol{\phi}_i(\boldsymbol{\xi}) := \prod_{j=1}^{3} \sin\left(\frac{a_{ij}\pi\xi_j}{L_{\xi_j}} + r_{ij}\right)\mathbf{e}_{q(i)} \tag{25}$$

imposing the following orthogonality property:

$$\int_{\mathcal{V}} \boldsymbol{\phi}_i(\boldsymbol{\xi})\cdot\boldsymbol{\phi}_k(\boldsymbol{\xi})\mathrm{d}\boldsymbol{\xi} = \delta_{ik} \tag{26}$$

In Eq. 25, $\{a_{ij}\}_{j=1}^{3}\in\mathbb{R}$ define the order of the function along $j$-th axis; $\{r_{ij}\}_{j=1}^{3}\in\mathbb{R}$ are the corresponding spatial phases; $\{L_{\xi_j}\}_{j=1}^{3}$ are the hyper-rectangle edge lengths; $\mathbf{e}_{q(i)}$ is a unit vector. Shape modifications can be applied along $\xi_1$, $\xi_2$, or $\xi_3$, with $q(i) = 1,2,$ or $3$ respectively.

On the one hand, GMF is independent of computational-grid topology. On the other hand, there is not a direct physical meaning associated to the shape modification.

## 4. Demonstration Application

The off-line dimensionality reduction method is applied for the shape reparameterization and hull-form optimization of the DTMB 5415 model (see Fig. 3).

**Table 2**
DTMB 5415 model scale main particulars and test condition.

| Description | Unit | Value |
|---|---|---|
| Displacement | tonnes | 0.549 |
| Length between perpendiculars | m | 5.720 |
| Beam | m | 0.760 |
| Draft | m | 0.248 |
| Longitudinal center of gravity | m | 2.884 |
| Vertical center of gravity | m | 0.056 |
| Water density | $\mathrm{kg/m^3}$ | 998.5 |
| Kinematic viscosity | $\mathrm{m^2/s}$ | 1.09E-06 |
| Gravity acceleration | $\mathrm{m/s^2}$ | 9.803 |
| Froude number | – | 0.280 |

**Figure 3:** A 5.720 m length model of the DTMB 5415 (CNR-INSEAN model 2340).

Main particulars of the model scale and optimization condition are summarized in Tab. 2. Since no rudder is considered here, the length between perpendiculars ($L_{\mathrm{pp}}$) is calculated from the fore perpendicular to the transom bottom edge.

### 4.1. Optimization Problem

The problem formulation for the shape optimization of the DTMB 5415 reads

$$\begin{array}{rll} \text{minimize} & R_{\mathrm{T}}(\mathbf{u}) & \text{with } \mathbf{u} \in \mathbb{R}^M \\ \text{subject to} & L_{\mathrm{pp}}(\mathbf{u}) = L_{\mathrm{pp}_0} & \\ \text{and to} & \nabla(\mathbf{u}) = \nabla_0, & \\ & |\Delta B(\mathbf{u})| \leq 0.05 B_0, & \\ & |\Delta T(\mathbf{u})| \leq 0.05 T_0, & \\ & V(\mathbf{u}) \geq V_0, & \\ & u_i^l \leq u_i \leq u_i^u & \forall i = 1, \dots, M \end{array} \tag{27}$$

where $R_{\mathrm{T}}$ is the calm-water resistance at $\mathrm{Fr} = 0.28$ (equivalent to 20 kn for the full-scale ship). Equality constraints are defined for the length between perpendiculars ($L_{\mathrm{pp}}$) and for the displacement ($\nabla$). Inequality constraints include 5% of maximum variation of beam ($B$) and the drought ($T$) and dedicated volume for the sonar dome ($V$), corresponding to 4.9 m diameter and 1.7 m length (cylinder). Subscript '0' indicates original-geometry values. Equality and inequality constraints on the geometry deformations are based on Diez et al. (2018b)

Using the reduced-dimensionality design space, the optimization problem (Eq. 27) is recast as

$$\begin{array}{rll} \text{minimize} & R_{\mathrm{T}}(\mathbf{x}) & \text{with } \mathbf{x} \in \mathbb{R}^N \\ \text{subject to} & L_{\mathrm{pp}}(\mathbf{x}) = L_{\mathrm{pp}_0} & \\ \text{and to} & \nabla(\mathbf{x}) = \nabla_0, & \\ & |\Delta B(\mathbf{x})| \leq 0.05 B_0, & \\ & |\Delta T(\mathbf{x})| \leq 0.05 T_0, & \\ & V(\mathbf{x}) \geq V_0, & \\ & x_i^l \leq x_i \leq x_i^u & \forall i = 1, \dots, N \end{array} \tag{28}$$

with $x_i^l = \inf\{\mathbf{z}_i^{\mathsf{T}}\mathbf{D}\}$ and $x_i^u = \sup\{\mathbf{z}_i^{\mathsf{T}}\mathbf{D}\}$.

### 4.2. Design-spaces Setup and Data Preprocessing

Three design spaces are used based on FFD, RBF, and GMF, defined by $M = 100$, 25, and 27 design variables, respectively. Details of shape modification parameters setup are summarized in Tabs. 3, 4, and 5. Figures 4a and b show, respectively, the FFD and

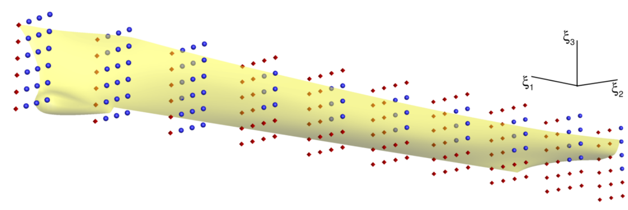

(a) Design space 1, FFD control points

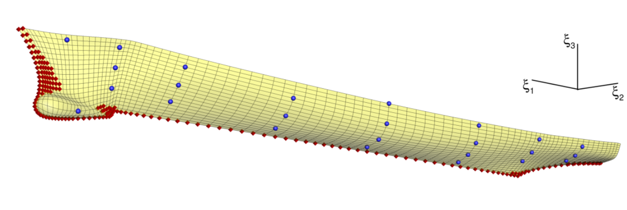

(b) Design space 2, RBF control points

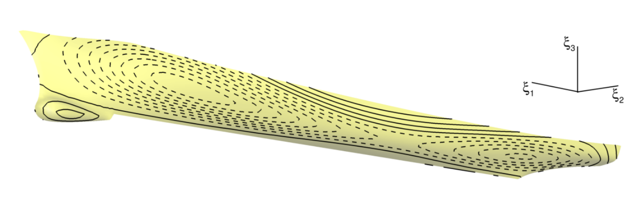

(c) Design space 3, GMF example modification (isomodification curves)

**Figure 4:** Shape modification methods at a glance.

RBF control points: blue dots represent (active) CPs whose coordinates are modified during the optimization, whereas red octahedra represents CPs with fixed coordinates. The latter are used to constrain the shape modification at the intersection with the symmetry plane ($\xi_2 = 0$). The number and the coordinates of CPs are chosen to generate global modifications of the hull. Finally, an example of the modification obtained by GMF is shown Fig. 4c. For all the methods, shape modifications are defined to produce geometry deformation in $\xi_2$-direction (direction perpendicular to the symmetry plane) only.

The number of design variables is chosen based on the quality of the shape modification obtained by each method. Different methods use different number of design variables. The design variables bounds (see Tabs. 3, 4, and 5) are set considering the trade-off between: (a) producing a meaningful and regular shape and (b) allowing shape modification variability as large as possible. Finally, to satisfy the equality constraints in Eq. 27, the following scaling equations are applied to the modified shapes:

$$\xi_1' = \xi_1' \frac{L_{\mathrm{pp}_0}}{L_{\mathrm{pp}}},$$

$$\xi_2' = \xi_2' \sqrt{\frac{\nabla_0}{\nabla} \frac{L_{\mathrm{pp}}}{L_{\mathrm{pp}_0}}},$$

**Table 3**
Design space 1, FFD control points and variables setup.

| Layer | Layer plane | No. CPs | No. active CPs | CPs activation criteria | Variable range |
|---|---|---|---|---|---|
| 1 | $\xi_1 = 0.00$ | 24 | 8 | $\xi_2 \geq 6.50 \wedge \xi_3 \geq 2.83$ | $-1.0 \leq \mathbf{u} \leq 1.0$ |
| 2 | $\xi_1 = 16.18$ | 24 | 8 | $\xi_2 \geq 6.50 \wedge \xi_3 \geq 2.83$ | $-1.0 \leq \mathbf{u} \leq 1.0$ |
| 3 | $\xi_1 = 32.37$ | 24 | 6 | $\xi_2 \geq 6.50 \wedge 2.83 \leq \xi_3 \leq 8.70$ | $-2.0 \leq \mathbf{u} \leq 2.0$ |
| 4 | $\xi_1 = 48.56$ | 24 | 6 | $\xi_2 \geq 6.50 \wedge 2.83 \leq \xi_3 \leq 8.70$ | $-2.0 \leq \mathbf{u} \leq 2.0$ |
| 5 | $\xi_1 = 64.75$ | 24 | 6 | $\xi_2 \geq 6.50 \wedge 2.83 \leq \xi_3 \leq 8.70$ | $-2.0 \leq \mathbf{u} \leq 2.0$ |
| 6 | $\xi_1 = 80.94$ | 24 | 6 | $\xi_2 \geq 6.50 \wedge 2.83 \leq \xi_3 \leq 8.70$ | $-2.0 \leq \mathbf{u} \leq 2.0$ |
| 7 | $\xi_1 = 97.13$ | 24 | 6 | $\xi_2 \geq 3.25 \wedge 2.83 \leq \xi_3 \leq 8.70$ | $-2.0 \leq \mathbf{u} \leq 2.0$ |
| 8 | $\xi_1 = 113.22$ | 24 | 18 | $\xi_2 \geq 3.25$ | $-1.0 \leq \mathbf{u} \leq 1.0$ |
| 9 | $\xi_1 = 129.51$ | 24 | 18 | $\xi_2 \geq 3.25$ | $-1.0 \leq \mathbf{u} \leq 1.0$ |
| 10 | $\xi_1 = 145.70$ | 24 | 18 | $\xi_2 \geq 3.25$ | $-1.0 \leq \mathbf{u} \leq 1.0$ |

**Table 4**
Design space 2, RBF control points and variables setup.

| Kernel | Shape parameter | No. CPs | No. active CPs | Variable range |
|---|---|---|---|---|
| Gaussian | $\epsilon = 1 \div 6$ | 207 | 25 | $-1.5 \leq \mathbf{u} \leq 1.5$ |

**Table 5**
Design space 3, GMF parameters and variables setup

| Function $i$ | $a_{i1}$ | $r_{i1}$ | $a_{i2}$ | $r_{i2}$ | $a_{i3}$ | $r_{i3}$ | $q(i)$ | Variable range |
|---|---|---|---|---|---|---|---|---|
| 1 | 1.0 | 0 | 1.0 | 0 | 1.0 | 0 | 2 | |
| 2 | 1.0 | 0 | 1.0 | 0 | 2.0 | 0 | 2 | |
| 3 | 1.0 | 0 | 2.0 | 0 | 1.0 | 0 | 2 | |
| 4 | 2.0 | 0 | 1.0 | 0 | 1.0 | 0 | 2 | |
| 5 | 1.0 | 0 | 2.0 | 0 | 2.0 | 0 | 2 | |
| 6 | 2.0 | 0 | 1.0 | 0 | 2.0 | 0 | 2 | |
| 7 | 2.0 | 0 | 2.0 | 0 | 1.0 | 0 | 2 | |
| 8 | 2.0 | 0 | 2.0 | 0 | 2.0 | 0 | 2 | |
| 9 | 1.0 | 0 | 1.0 | 0 | 3.0 | 0 | 2 | |
| 10 | 1.0 | 0 | 3.0 | 0 | 1.0 | 0 | 2 | |
| 11 | 3.0 | 0 | 1.0 | 0 | 1.0 | 0 | 2 | |
| 12 | 1.0 | 0 | 2.0 | 0 | 3.0 | 0 | 2 | |
| 13 | 2.0 | 0 | 1.0 | 0 | 3.0 | 0 | 2 | |
| 14 | 1.0 | 0 | 3.0 | 0 | 2.0 | 0 | 2 | $-1.0 \leq \mathbf{u} \leq 1.0$ |
| 15 | 2.0 | 0 | 3.0 | 0 | 1.0 | 0 | 2 | |
| 16 | 3.0 | 0 | 1.0 | 0 | 2.0 | 0 | 2 | |
| 17 | 3.0 | 0 | 2.0 | 0 | 1.0 | 0 | 2 | |
| 18 | 2.0 | 0 | 2.0 | 0 | 3.0 | 0 | 2 | |
| 19 | 2.0 | 0 | 3.0 | 0 | 2.0 | 0 | 2 | |
| 20 | 3.0 | 0 | 2.0 | 0 | 2.0 | 0 | 2 | |
| 21 | 1.0 | 0 | 3.0 | 0 | 3.0 | 0 | 2 | |
| 22 | 3.0 | 0 | 1.0 | 0 | 3.0 | 0 | 2 | |
| 23 | 3.0 | 0 | 3.0 | 0 | 1.0 | 0 | 2 | |
| 24 | 2.0 | 0 | 3.0 | 0 | 3.0 | 0 | 2 | |
| 25 | 3.0 | 0 | 2.0 | 0 | 3.0 | 0 | 2 | |
| 26 | 3.0 | 0 | 3.0 | 0 | 2.0 | 0 | 2 | |
| 27 | 3.0 | 0 | 3.0 | 0 | 3.0 | 0 | 2 | |

$$\xi_3' = \frac{(\xi_3' + T_0)\frac{\nabla_0}{\nabla}}{\frac{L_{\mathrm{pp}0}}{L_{\mathrm{pp}}}\frac{B_0}{B_0}} - T_0 \tag{29}$$

Moreover, designs not satisfying the inequality constraints in Eq. 27 are not included in the data matrix (see Eq. 7). As a results, all designs processed by PCA are feasible. The idea is to define an optimal basis for the representation of the feasible domain. Nevertheless, there are no guarantees that all geometries are feasible during the optimization.

The design spaces are sampled following a uniform random distribution of $S = 40,000$ hull-form designs by the MC method. The data matrix $\mathbf{D}$ collects a $L = 1,800$ grids points from hull discretization. The design spaces feasibility (with respect to geometric constraints) is shown in Tab. 6. Design space 3 (based on GMF) has the highest feasibility (16.5%), followed by design space 2 (based on RBF) (12.6%), whereas the design space 1 (based on FFD) achieves the lowest number of feasible geometries (6.4%). Finally, a subset of 2,000 feasible designs is randomly selected (no bias is introduced). They are used to define the design-spaces data matrices (with dimension $2,000 \times 1,800$) and compare the results.

**Table 6**
Design-space feasibility (F) based on 40,000 Monte Carlo samples.

| Design space | No. feasible shapes | F% |
|---|---|---|
| 1 (FFD) | 2,579 | 6.40 |
| 2 (RBF) | 5,078 | 12.6 |
| 3 (GMF) | 6,653 | 16.5 |

### 4.3. Hydrodynamic Solver

The calm-water total resistance is evaluated using the linear potential flow code WARP (Wave Resistance Program), developed at CNR-INM. Wave resistance computations are based on the Dawson (double-model) linearization (Dawson, 1977). The frictional resistance is estimated using a flat-plate approximation, based on the local Reynolds number (Schlichting and Gersten, 2000). The ship balance (sinkage and trim) is fixed. Details of equations, numerical implementations, and validation of the numerical solver are given in Bassanini et al. (1994). Simulations are performed for the right demi-hull, taking advantage of symmetry about the $\xi_1\xi_3$-plane. The computational domain for the free-surface is defined within $1L_{\rm pp}$ upstream, $3L_{\rm pp}$ downstream, and $1.5L_{\rm pp}$ sideways, for a total of $150\times44$ grid nodes. The associated hull grid if formed by $180 \times 40$ nodes.

### 4.4. Optimization Algorithm and Setup

As global optimizer, a deterministic particle swarm optimization (DPSO, Serani et al. 2016b) is used. It is formulated as follows

$$\begin{cases} \mathbf{v}_j^{k+1} = \chi\left[\mathbf{v}_j^k + c_1(\mathbf{p}_j - \mathbf{x}_j^k) + c_2(\mathbf{g} - \mathbf{x}_j^k)\right] \\ \mathbf{x}_j^{k+1} = \mathbf{x}_j^k + \mathbf{v}_j^{k+1} \end{cases} \tag{30}$$

The above equations update velocity ($\mathbf{v}_j^k$) and position ($\mathbf{x}_j^k$) of the $j$-th particle at the $k$-th iteration, where: $\chi$ is the constriction factor; $c_1$ and $c_2$ are respectively the social and cognitive learning rate; $\mathbf{p}_j$ is the personal best position ever found by the $j$-th particle in the previous iterations and $\mathbf{g}$ is the global best position ever found in the previous iterations by all the particles. A discussion for an effective and efficient use of DPSO for SBDO in ship hydrodynamics has been presented in Serani and Diez (2017a). The parameter setup used for DPSO is selected as suggested in Serani et al. (2016b): number of particles $N_p = 4N$; particle initialization with Hammersley sequence sampling (HSS) distribution on domain only with non-null velocity; set of coefficients equal to $\chi = 0.721$, $c_1 = c_2 = 1.655$; semi-elastic wall-type approach for box constraints. A fixed and limited budget of 1,000 function evaluations is used.

## 5. Numerical Results

Design-space assessment and dimensionality reduction results, along with simulation-based optimization outcomes, are presented and discussed in the following subsections.

### 5.1. Design-space Assessment and Dimensionality Reduction

The design-space assessment and dimensionality reduction is based on the PCA eigenvalues and eigenvectors. The former identify the original design-space variability retained (see Eq. 10), whereas the latter define the reconstruction error through projection (see Eq. 13). Herein, the reduced-dimensionality $N$ is set so as to achieve a NMSE $\leq 5\%$, equivalent (at least) to the 95% of the original design-space variability. The reduced-dimensionality models are validated using a 10-fold cross-validation procedure (Ross, 2014). Training and test sets are composed by 90 and 10%, respectively, of the 2,000 MC items.

Figure 5 presents the variance retained by the first $N$ PCA eigenvectors, which equals the PCA eigenvalues cumulative sum. It can be seen how, with current settings and design-variable bounds, design space 3 (GMF) achieves the highest design variability, whereas design space 2 (RBF) achieves the lowest. Specifically, design space 3 achieves a geometric variance that is about twice and about one and a half times that obtained by design spaces 2 (RBF) and 1 (FFD), respec-

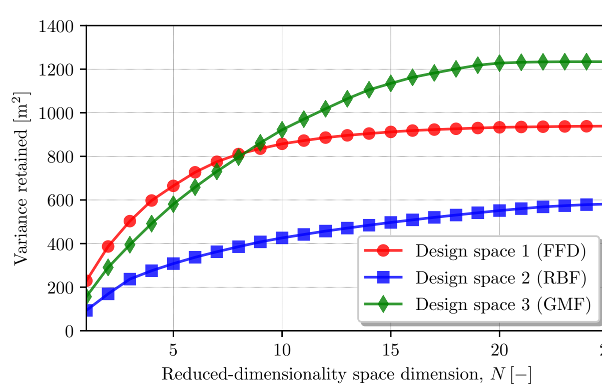


**Figure 5:** Design-space variability retained as a function of the number $N$ of PCA components.

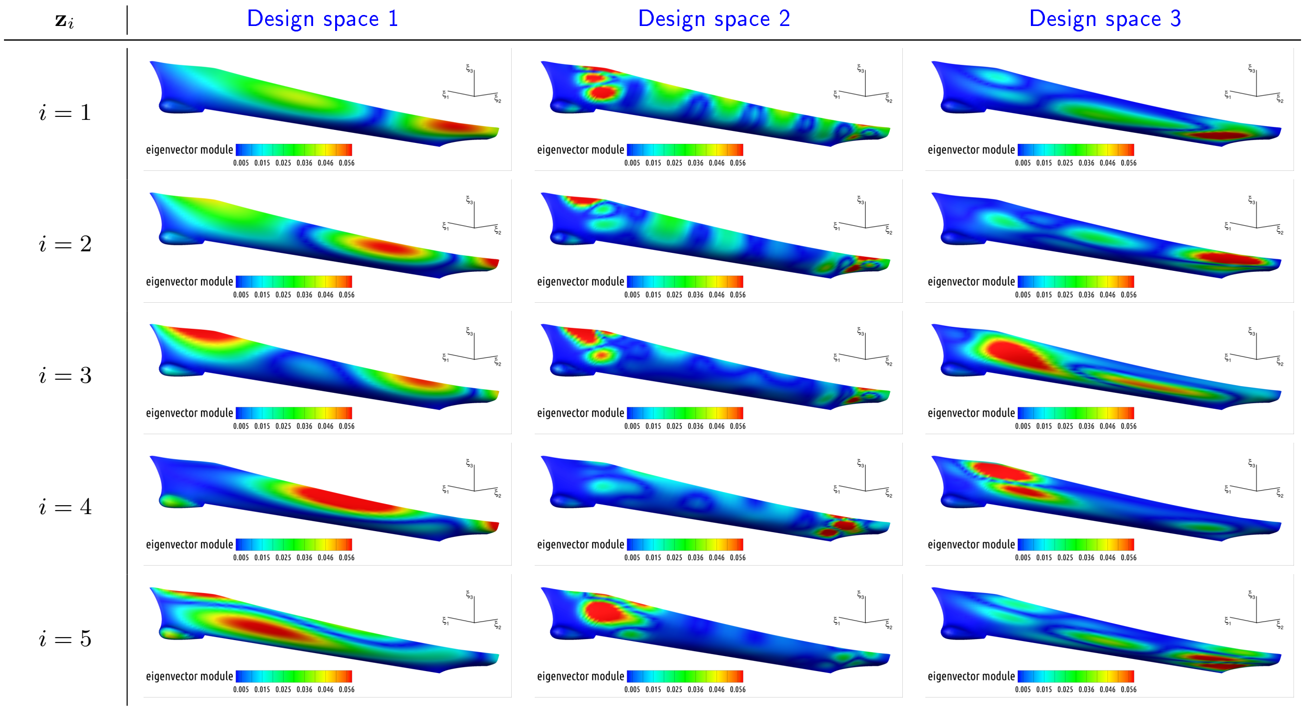


**Figure 6:** Module of the first five PCA eigenvectors.

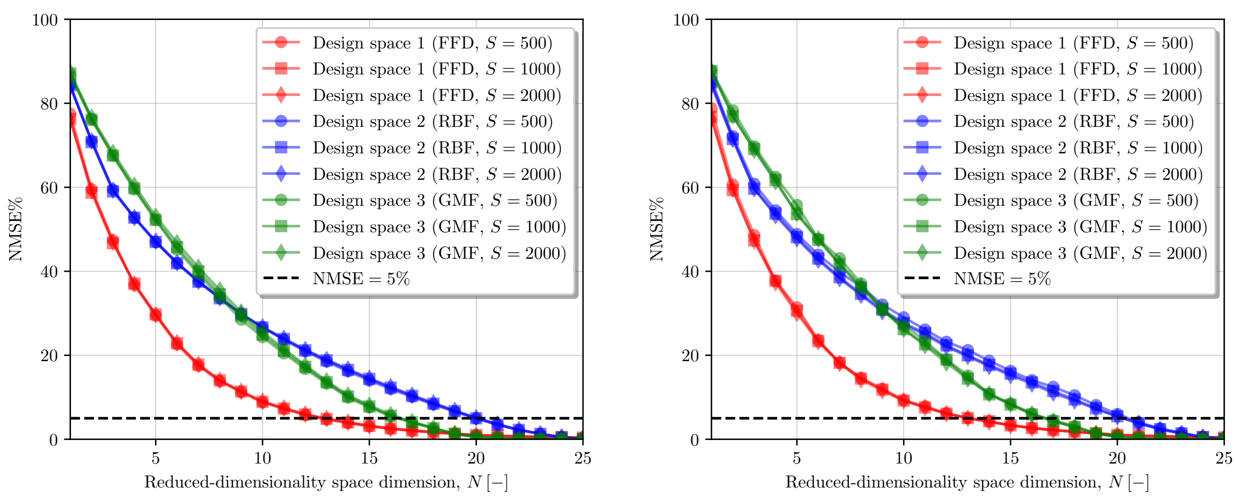


(a) Training set

(b) Test set

**Figure 7:** NMSE convergence as a function of the number $N$ of PCA components.

tively. This can be justified by the GMF formulation, since it is intrinsically global, whereas both FFD and RBF are local and limited by the number and position of CPs. First five PCA eigenvectors are shown in Fig. 6, for each design space. Specifically, the most important eigenvectors for each design-space parameterization show the type and order of variations addressed with each design space. This comparison emphasizes the difference in variations produced by the different design spaces. For instance, the setup for design spaces 1 and 3 (based on the current implementation of FFD and GMF, respectively) provides with more global shape modifications with significant variations in sectional area and waterline along the ship length. The design space 2 (based on RBF) gives more localized modifications close to the bow and the stern.

The design-space dimensionality reduction convergence versus the number of MC samples ($S$) is shown in Fig. 7 in terms of NMSE as a function of the reduced-dimensionality space dimension $N$. Training and test sets results are shown in Fig. 7a and b, respectively. The results are found convergent versus $S$ for all the

**Table 7**
Dimensionality reduction (DR) summary.

| Design space | Parameterization | No. design variables Original ($M$) | No. design variables Reduced ($N$) | DR% | NMSE% Training set | NMSE% Test set |
|---|---|---|---|---|---|---|
| 1 | FFD | 100 | 14 | 86 | 4.03 | 4.12 |
| 2 | RBF | 25 | 21 | 16 | 3.62 | 3.78 |
| 3 | GMF | 27 | 17 | 37 | 4.20 | 4.34 |

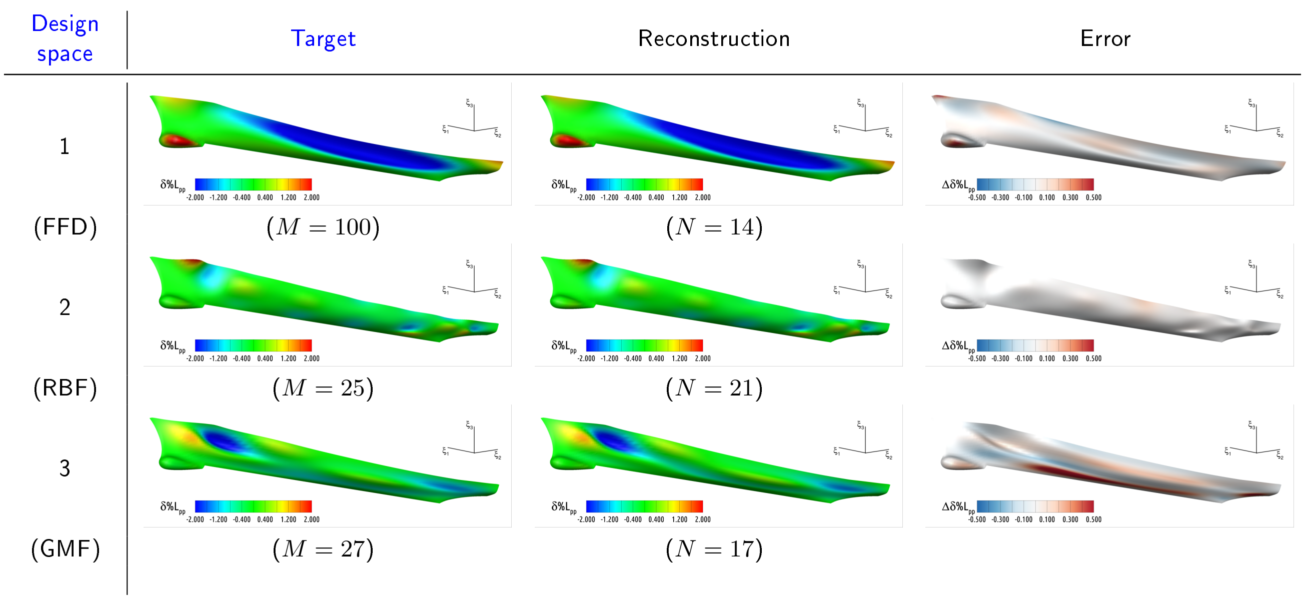


**Figure 8**: Example of reconstruction and error of three target hull variants.

shape modification methods. The three design spaces have been reduced up to $N = 14$ (design space 1), 21 (design space 2), and 17 (design space 3) design variables, respectively. The design space 1 (based on FFD) shows the highest dimensionality reduction (86%), followed by the design space 3 (based on GMF, 37%), and finally the design space 2 (based on RBF, 16%). Shape reparameterization results are summarized in Tab. 7. An example of shape reconstruction of a target geometry (one of the 2,000 MC items) and the corresponding reconstruction error using the reduced-dimensionality design spaces is shown in Fig. 8. For each design space, the target geometry is quite extreme and not realistic, and used as challenging test for demonstration. No significant differences between target and reconstructed hulls can be observed, with low values of the reconstruction error.

Based on the current design-spaces setup, the results underline that: (1) overall, the GMF method is capable to provide the highest design-space variance (see Fig. 5), (2) the FFD method defines a highly-linearly dependent design-space, since it achieves a significant dimensionality reduction (see Tab. 7). Finally, GMF and RBF (relatively) low dimensionality-reduction values show the difficulty to reduced the design-space dimensionality, if the original space is suitably "well-defined". This means that independently of the shape modification method, if the original design space is defined by a basis of linearly-independent shape modification vectors, the KLE/PCA cannot provide with any dimensionality reduction.

## 5.2. Optimization

To assess the effects of the reduced-dimensionality spaces on the hull-form optimization of the DTMB 5415 three analysis are carried out for each design space: (1)

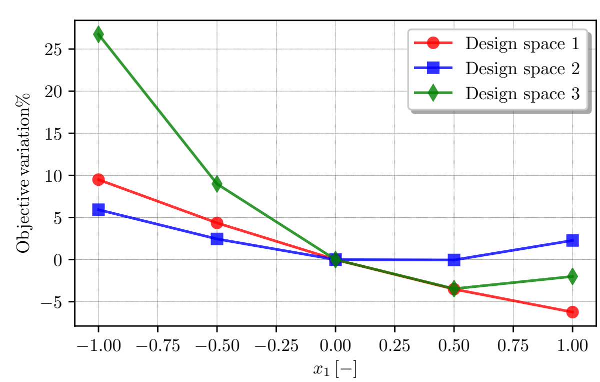


**Figure 9**: Sensitivity analysis conditional to 1st PCA eigenvector.

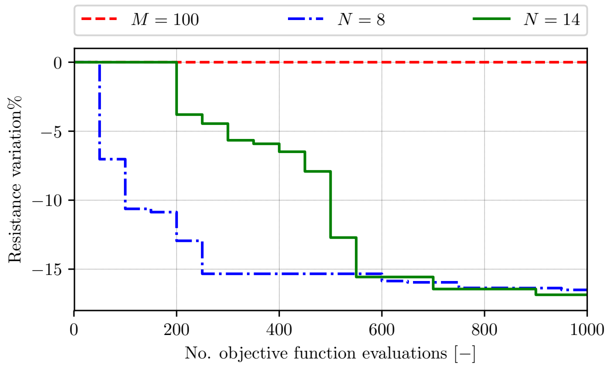


(a) Design space 1

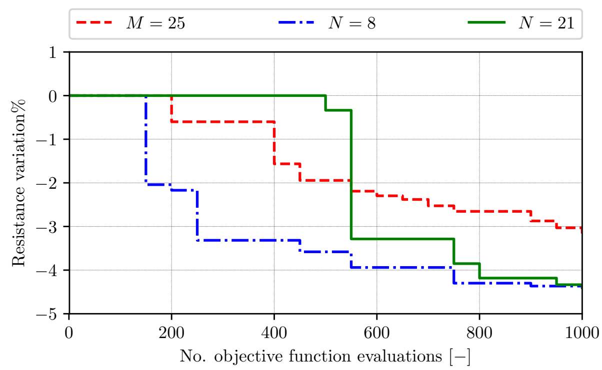


(b) Design space 2

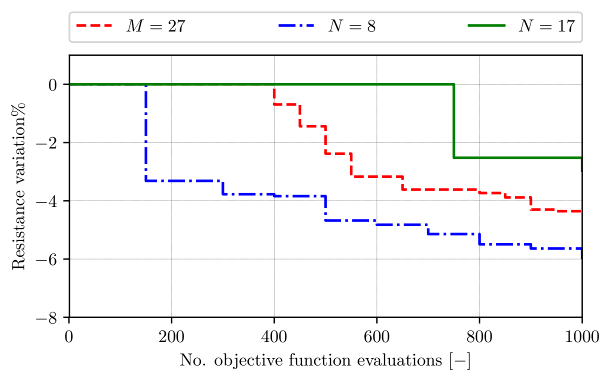


(c) Design space 3

**Figure 10:** Optimization convergence conditional to design space parameterization.

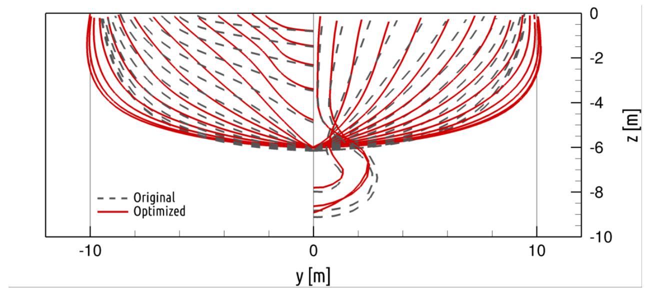


(a) Design space 1, $N = 14$

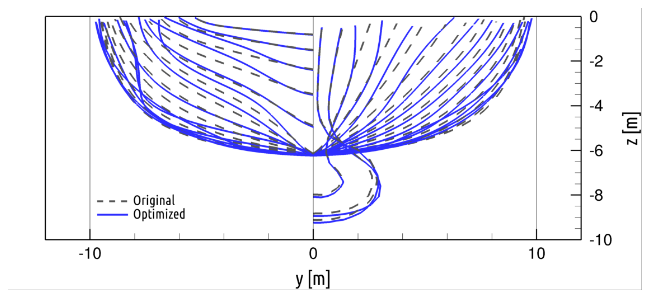


(b) Design space 2, $N = 21$

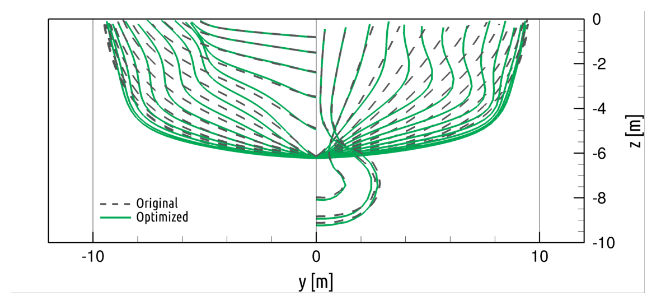


(c) Design space 3, $N = 8$

**Figure 11:** Original versus optimized shapes.

a preliminary sensitivity analysis along the 1st PCA eigenvector; (2) an SBDO procedure using two reduced-dimensionality design spaces with $N = 8$ and the value providing NMSE $\leq 5\%$, respectively; (3) an SBDO procedure using the original design space.

The sensitivity analysis along the 1st PCA eigenvector is shown in Fig. 9. The reduced-design variable $x_1$ is normalized between -1 and 1. The design space 1 provides the highest objective improvement (about 6%) followed by design space 3 (3.5%), whereas design space 2 produces an improvement lower than 0.1%. These is in agreement with the results of the design-spaces assessment: the improvement ranking corresponds to the variance-retained (by 1st PCA eigenvector) ranking (see Fig. 5).

Figure 10 shows the comparison of the optimization convergence conditional to the design space, using two reduced-dimensionality spaces and the original one: $N = 8$, 14 and $M = 100$ for design space 1; $N = 8$, 21 and $M = 25$ for design space 2; $N = 8$, 17 and $M = 27$ for design space 3. Shape reparameterization by reduced-dimensionality spaces provides a larger objective improvement than the original design space, except for design space 3 with $N = 17$. It may be noted that the optimization runs are performed using a fixed (and intentionally limited) budget of function evaluations, meaning that the optimization algorithm is far from the convergence. A comparison of the design-space-best optima hull stations and wave elevation ($\eta$) patterns to the original is shown in Figs. 11 and 12. The highest resistance reduction, achieved by the design space 1 ($N = 14$), can be associated with a significant modification/reduction of the sonar dome area (see Fig. 11a) and a reduction of both diverging

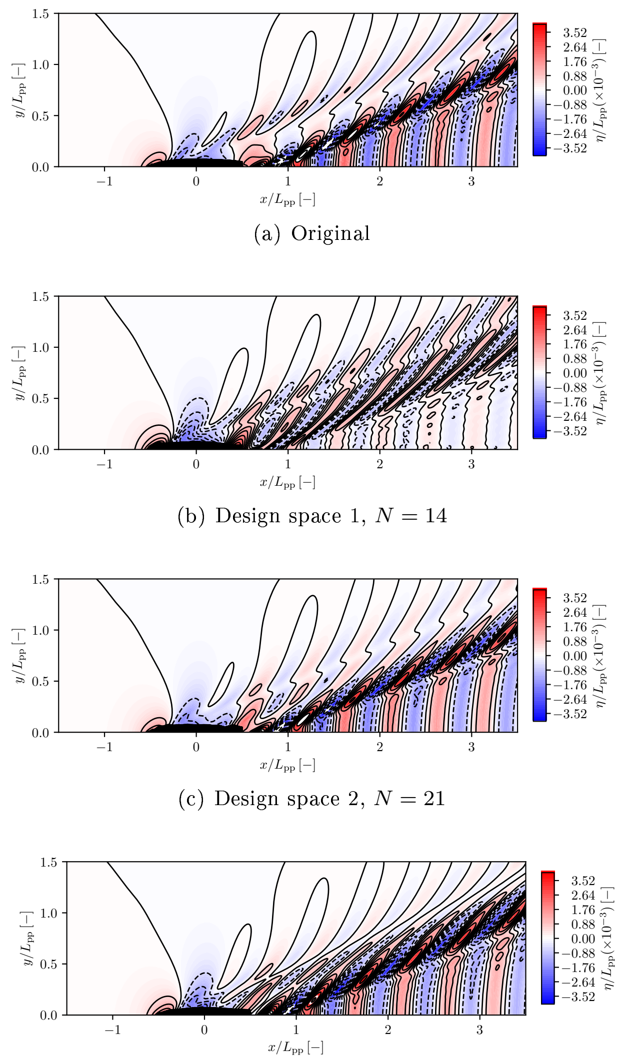


(a) Original

(b) Design space 1, $N = 14$

(c) Design space 2, $N = 21$

(d) Design space 3, $N = 8$

**Figure 12:** Original versus optimized wave elevation patterns.

and transverse stern waves (see Fig. 12b). The optimization results are summarized in Tab. 8.

Finally, Fig. 13 shows the resistance reduction as a function of the geometric-variance retained by each design space. Its linear regression (LR) show how the resistance decreases as the geometric variance increases. Nevertheless, considering different design spaces, a greater geometric variability is not always associated with a greater improvement of the objective function. This can be justified by the absence of physic-based information in the dimensionalty-reduction procedure, which is based on geometric variables only. It can be also noted how the FFD search for global optimum with 100 design variables consumes the entire evaluation budget without achieving any objective improvement. Nevertheless, its reduced-dimensionality space with $N = 14$ and almost the same geometric variance achieves the best design overall, highlighting the potentiality of the method.

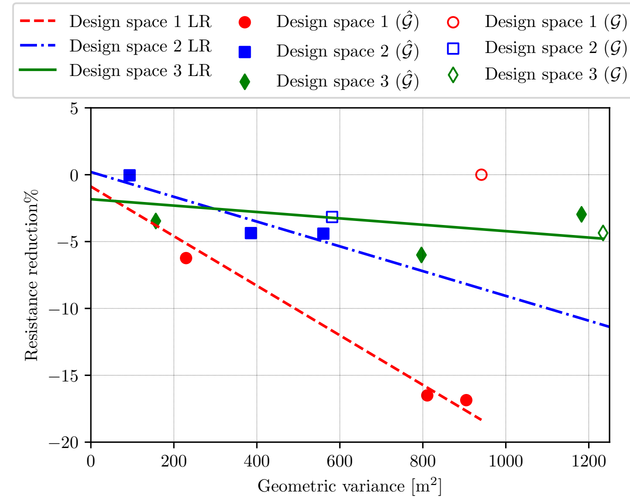


**Figure 13:** Linear regression (LR) of the objective improvement as function of the geometric variance retained by the reduced design spaces ($\hat{\mathcal{G}}$).

**Table 8**
Optimization results summary in terms of model-scale resistance reduction at $\mathrm{Fr} = 0.28$.

| No. evaluations | Design space 1 | Design space 2 | Design space 3 |
|---|---|---|---|
| 4 | -6.23% ($N = 1$) | -0.05% ($N = 1$) | -3.46% ($N = 1$) |
| 1000 | -16.5% ($N = 8$) | -4.37% ($N = 8$) | -6.00% ($N = 8$) |
| 1000 | -16.9% ($N = 14$) | -4.41% ($N = 21$) | -2.96% ($N = 17$) |
| 1000 | 0.00% ($M = 100$) | -3.16% ($M = 25$) | -4.36% ($M = 27$) |

## 6. Conclusions and Future Work

A method based on the Karhunen-Loève expansion has been formulated for the assessment of arbitrary design spaces in shape optimization, assessing the shape modification variability and providing the definition of a reduced-dimensionality global model of the shape modification vector. The method is based on the concept of geometric variance and does not require simulations and/or design performance analyses. At the continuous level, the KLE is applied to the continuous shape modification vector, assuming stochastic design variables. At the discrete level, the problem reduces to the PCA of a discrete set of geometrical data. Specifically, the KLE problem is formulated in the continuous domain and reduces to the eigenproblem of an integral operator, representing a Fredholm integral equation of the second kind. The discretization of the shape domain (and associated integral equation) yields the eigenproblem of a matrix, which appears to be the autocovariance matrix of the discretized shape modification vector. Finally, this corresponds to solving the PCA of the discretized shape modification vector.

The present work has demonstrated how the method can be used to assess different design spaces and shape parameterization methods before optimization is performed and without the need of running simulations for the performance prediction and/or its gradient. The method has been further used to reduce the dimensionality of design spaces (based on KLE/PCA eigenvalues), providing a shape reparameterization using KLE/PCA eigenmodes. These are finally used for simulation-based design optimization, aiming at global optimum.

A demonstration for the hull-form optimization of the DTMB 5415 model in calm water has been discussed, where three design spaces were investigated. These were provided by FFD, RBF, and GMF. With current settings, FFD, RBF, and GMF design-space dimensionality was reduced by 86, 16, and 37%, respectively, allowing for a NMSE of 5% (corresponding to the 95% of reconstructed geometric variance). Current results have shown the effectiveness of the method in defining efficient design spaces. Under the assumption of limited budget of function evaluations (as often encountered in SBDO problems), reduced-dimensionality spaces have achieved, in general, larger objective improvements than the original parameterizations. Specifically, the latter have provided 0% (design space 1, FFD), 3.2% (design space 2, RBF), and 4.4% (design space 3, GMF) resistance reduction, whereas reduced-dimensionality spaces have given 17% (design space 1), 4.4% (design space 2), and 6% (design space 3). It is a notable result that the global optimization algorithm is not able to provide with any objective improvement using the original FFD method with $M = 100$ design variables. The design-space dimensionality reduction of the FFD parameterization reduced the number of design variables to $N = 14$ and drove the global optimizer to the best overall optimum among all cases studied here (Fig. 13).

In general it may be noted that the geometric variance is not always proportional to the objective variation or improvement. Therefore, it is not straightforward to state (based on the geometric variance only) whether a parameterization method (with associated setup) is better than another one or not in the search for a global optimum. For instance, design space 3 have provided the highest design variability/feasibility, but this was not associated to the largest objective improvement, which was achieved by design space 1. These results show how the process of defining an efficient and effective design-space can be complex and how a proper definition of the shape modification method is always advisable.

The method presented goes beyond the current application and is suitable in all areas where shape design is of primary importance (such as aerodynamics, structural, and heat transfer applications), involving complex single- and multi-disciplinary simulations facing multiple environmental and operating conditions.

Finally, it may noted that significant physical phenomena induced by small shape modifications (such as transitions, separations, etc.) may be overlooked as no physical information is processed by the method, which justifies that retaining a large geometric variance is not always associated to achieving better objective function values. The inclusion of physics-based information in the dimensionality-reduction formulation has been presented and discussed in Diez et al. (2016b); Serani et al. (2017); Serani and Diez (2018b) and part of ongoing research. Furthermore, linear methods such as KLE/PCA may not be efficient when a complex non-linear relationship between design variables are involved. The extension to non-linear dimensionality reduction methods and their effects on shape optimization have been discussed in D'Agostino et al. (2018a,b), and D'Agostino et al. (2018c). The use of non-linear methods with combined geometry and physics-based data has been presented in D'Agostino et al. (2019); Serani et al. (2019) and subject of ongoing studies.

## Acknowledgments

This work was partially supported by the US Department of the Navy Office of Naval Research Global, NICOP grant N62909-18-1-2033, administered by Dr. Salahuddin Ahmed and Dr. Woei-Min Lin, and by the Italian Flagship Project RITMARE, funded by the Italian Ministry of Education, University, and Research.

## References

Barr, A.H., 1984. Global and local deformations of solid primitives. SIGGRAPH Comput. Graph. 18, 21–30.

Bassanini, P., Bulgarelli, U., Campana, E.F., Lalli, F., 1994. The wave resistance problem in a boundary integral formulation. Surveys on Mathematics for Industry 4, 151–194.

Bletzinger, K.U., Maute, K., 1997. Towards generalized shape and topology optimization. Engineering Optimization 29, 201–216.

Bloor, M.I.G., Wilson, M.J., 1995. Efficient parameterization of genetic aircraft geometry. Journal of Aircraft 32, 1269–1275.

Borzì, A., Schulz, V., Schillings, C., Von Winckel, G., 2010. On the treatment of distributed uncertainties in pde-constrained optimization. GAMM-Mitteilungen 33, 230–246.

Campana, E.F., Diez, M., Iemma, U., Liuzzi, G., Lucidi, S., Rinaldi, F., Serani, A., 2015. Derivative-free global ship design optimization using global/local hybridization of the DIRECT algorithm. Optimization and Engineering 17, 127–156.

Campana, E.F., Liuzzi, G., Lucidi, S., Peri, D., Piccialli, V., Pinto, A., 2009a. New global optimization methods for ship design problems. Optimization and Engineering 10, 533–555.

Campana, E.F., Peri, D., Tahara, Y., Kandasamy, M., Stern, F., 2009b. Numerical optimization methods for ship hydrodynamic design. Transactions - Society of Naval Architects and Marine Engineers Society of Naval Architects and Marine Engineers , 30–67.

Campana, E.F., Peri, D., Tahara, Y., Stern, F., 2006. Shape optimization in ship hydrodynamics using computational fluid dynamics. Computer methods in applied mechanics and engineering 196, 634–651.

Chen, X., Diez, M., Kandasamy, M., Zhang, Z., Campana, E.F., Stern, F., 2015. High-fidelity global optimization of shape design by dimensionality reduction, metamodels and deterministic particle swarm. Engineering Optimization 47, 473–494.

D'Agostino, D., Serani, A., Campana, E.F., Diez, M., 2018a. Deep autoencoder for off-line design-space dimensionality reduction in shape optimization, in: 56th AIAA Aerospace Sciences Meeting, SciTech 2018, Gaylord Palms, Kissimmee, Florida, USA, January 8-12.

D'Agostino, D., Serani, A., Campana, E.F., Diez, M., 2018b. Nonlinear methods for design-space dimensionality reduction in shape optimization, in: Nicosia, G., Pardalos, P., Giuffrida, G., Umeton, R. (Eds.), Machine Learning, Optimization, and Big Data. MOD 2017. Lecture Notes in Computer Science, vol 10710, Springer International Publishing, Cham. pp. 121–132.

D'Agostino, D., Serani, A., Campana, E.F., Diez, M., 2019. Augmented design-space exploration by nonlinear dimensionality reduction methods, in: Nicosia, G., Pardalos, P., Giuffrida, G., Umeton, R., Sciacca, V. (Eds.), Machine Learning, Optimization, and Data Science. LOD 2018. Lecture Notes in Computer Science, vol 11331, Springer International Publishing, Cham. pp. 154–165.

D'Agostino, D., Serani, A., Diez, M., 2018c. On the combined effect of design-space dimensionality reduction and optimization methods on shape optimization efficiency, in: 19th AIAA/ISSMO Multidisciplinary Analysis and Optimization Conference (MA&O), AVIATION 2018, Atlanta, GA, USA, June 25-29.

Dawson, C.W., 1977. A practical computer method for solving ship-wave problems, in: Proceedings of the 2nd International Conference on Numerical Ship Hydrodynamics, Berkeley. pp. 30–38.

Diez, M., Campana, E.F., Stern, F., 2015a. Design-space dimensionality reduction in shape optimization by Karhunen–Loève expansion. Computer Methods in Applied Mechanics and Engineering 283, 1525–1544.

Diez, M., Campana, E.F., Stern, F., 2015b. Development and evaluation of hull-form stochastic optimization methods for resistance and operability, in: Proceedings of the 13th International Conference on Fast Sea Transportation, FAST 2015, Washington, D.C., USA.

Diez, M., Campana, E.F., Stern, F., 2018a. Stochastic optimization methods for ship resistance and operational efficiency via cfd. Structural and Multidisciplinary Optimization 57, 735–758.

Diez, M., Serani, A., Campana, E.F., Stern, F., 2018b. Assessing the Ability to Optimize Hull Forms of Sea Vehicles for Best Performance in a Sea Environment, STO-TR-AVT-204, Chapter 3: INSEAN/UI Optimization Approach. Technical Report. NATO.

Diez, M., Serani, A., Campana, E.F., Stern, F., 2018c. Stochastic Design Optimization for Naval and Aero Military Vehicles, STO-TR-AVT-252, Chapter 7: Reliability-Based Robust Hull-Form Optimization of a Naval Destroyer in Waves. Technical Report. NATO.

Diez, M., Serani, A., Campana, E.F., Volpi, S., Stern, F., 2016a. Design space dimensionality reduction for single- and multidisciplinary shape optimization, in: AIAA/ISSMO Multidisciplinary Analysis and Optimization (MA&O), AVIATION 2016, Washington D.C., USA, June 13-17.

Diez, M., Serani, A., Stern, F., Campana, E.F., 2016b. Combined geometry and physics based method for design-space dimensionality reduction in hydrodynamic shape optimization, in: Proceedings of the 31st Symposium on Naval Hydrodynamics, Monterey, CA, USA.

Grigoropoulos, G.J., Chalkias, D.S., 2010. Hull-form optimization in calm and rough water. Computer-Aided Design 42, 977–984.

Haftka, R.T., Grandhi, R.V., 1986. Structural shape optimization-a survey. Computer Methods in Applied Mechanics and Engineering 57, 91–106.

Harries, S., Abt, C., 2019. Faster turn-around times for the design and optimization of functional surfaces. Ocean Engineering 193, 106470.

Hicks, R.M., Henne, P.A., 1978. Wing design by numerical optimization. Journal of Aircraft 15, 407–412.

Jones, D., Perttunen, C., Stuckman, B., 1993. Lipschitzian optimization without the Lipschitz constant. Journal of Optimization Theory and Applications 79, 157–181.

Kandasamy, M., Peri, D., Tahara, Y., Wilson, W., Miozzi, M., Georgiev, S., Milanov, E., Campana, E.F., Stern, F., 2013. Simulation based design optimization of waterjet propelled Delft catamaran. International Shipbuilding Progress 60, 277–308.

Leiva, J.P., Watson, B.C., 1998. Automatic generation of basis vectors for shape optimization in the GENESIS program, in: 7th AIAA/USAF/NASA/ISSMO Symposium on Multidisciplinary Analysis and Optimization Conference Proceedings, AIAA, pp. 1115–1122.

Lukaczyk, T., Palacios, F., Alonso, J.J., Constantine, P., 2014. Active subspaces for shape optimization, in: Proceedings of the 10th AIAA Multidisciplinary Design Optimization Specialist Conference, National Harbor, Maryland, USA, 13-17 January.

Menzel, S., Sendhoff, B., 2008. Evolutionary Computation in Practice. Springer Berlin Heidelberg, Berlin, Heidelberg. chapter Representing the Change - Free Form Deformation for Evolutionary Design Optimization. pp. 63–86.

Pickett Jr., R.M., Rubistein, M.F., Nelson, R.B., 1973. Automated structural synthesis using a reduced number of design coordinates. AIAA Journal 11, 489–494.

Poole, D.J., Allen, C.B., Rendall, T.C.S., 2017. High-fidelity aerodynamic shape optimization using efficient orthogonal modal design variables with a constrained global optimizer. Computers & Fluids 143, 1 – 15.

Raghavan, B., Breitkopf, P., Tourbier, Y., Villon, P., 2013a. Towards a space reduction approach for efficient structural shape optimization. Structural and Multidisciplinary Optimization 48, 987âĂŞ1000.

Raghavan, B., Xiang, L., Breitkopf, P., Rassineux, A., Villon, P., 2013b. Towards simultaneous reduction of both input and output spaces for interactive simulation-based structural design. Comput. Methods Appl. Mech. Engrg. 265, 174–185.

Ross, S.M., 2014. Introduction to Probability and Statistics for Engineers and Scientists. Fifth edition ed., Academic Press, Boston.

Rozvany, G.I., Zhou, M., Birker, T., 1992. Generalized shape optimization without homogenization. Structural optimization 4, 250–252.

Samareh, J.A., 2001. Survey of shape parameterization techniques for high-fidelity multidisciplinary shape optimization. AIAA journal 39, 877–884.

Schillings, C., Schmidt, S., Schulz, V., 2011. Efficient shape optimization for certain and uncertain aerodynamic design. Computers & Fluids 46, 78–87.

Schlichting, H., Gersten, K., 2000. Boundary-Layer Theory. Springer-Verlag, Berlin.

Sederberg, T.W., Parry, S.R., 1986. Free-form deformation of solid geometric models. ACM SIGGRAPH computer graphics 20, 151–160.

Serani, A., Campana, E.F., Diez, M., Stern, F., 2017. Towards augmented design-space exploration via combined geometry and physics based Karhunen-Loève expansion, in: 18th AIAA/ISSMO Multidisciplinary Analysis and Optimization Conference (MA&O), AVIATION 2017, Denver, USA, June 5-9.

Serani, A., D'Agostino, D., Campana, E.F., Diez, M., 2019. Assessing the interplay of shape and physical parameters by unsupervised nonlinear dimensionality reduction methods. Journal of Ship Research , 1–15In press.

Serani, A., Diez, M., 2017a. Are random coefficients needed in particle swarm optimization for simulation-based ship design?, in: Proceedings of the 7th International Conference on Computational Methods in Marine Engineering (Marine 2017).

Serani, A., Diez, M., 2017b. Dolphin Pod Optimization, in: Tan, Y., Takagi, H., Shi, Y. (Eds.), Advances in Swarm Intelligence. ICSI 2017. Springer, Cham. Lecture Notes in Computer Science, vol 10385, pp. 63–70.

Serani, A., Diez, M., 2018a. Dolphin pod optimization: A nature-inspired deterministic algorithm for simulation-based design, in: Nicosia, G., Pardalos, P., Giuffrida, G., Umeton, R. (Eds.), Machine Learning, Optimization, and Big Data. MOD 2017. Lecture Notes in Computer Science, vol 10710, Springer International Publishing, Cham.

Serani, A., Diez, M., 2018b. Shape optimization under stochastic conditions by design-space augmented dimensionality reduction, in: 19th AIAA/ISSMO Multidisciplinary Analysis and Optimization Conference (MA&O), AVIATION 2018, Atlanta, USA, June 25-29.

Serani, A., Fasano, G., Liuzzi, G., Lucidi, S., Iemma, U., Campana, E.F., Stern, F., Diez, M., 2016a. Ship hydrodynamic optimization by local hybridization of deterministic derivative-free global algorithms. Applied Ocean Research 59, 115 – 128.

Serani, A., Leotardi, C., Iemma, U., Campana, E.F., Fasano, G., Diez, M., 2016b. Parameter selection in synchronous and asynchronous deterministic particle swarm optimization for ship hydrodynamics problems. Applied Soft Computing 49, 313 – 334.

Sieger, D., Menzel, S., Botsch, M., 2014. RBF morphing techniques for simulation-based design optimization. Engineering with Computers 30, 161–174.

Sieger, D., Menzel, S., Botsch, M., 2015. New Challenges in Grid Generation and Adaptivity for Scientific Computing. Springer International Publishing, Cham. chapter On Shape Deformation Techniques for Simulation-Based Design Optimization. pp. 281–303.

Yang, X.S., 1995. Handbook of Solid Modeling. McGraw-Hill.